Plasmonics (2021) 16:1809–1816
https://doi.org/10.1007/s11468-020-01367-5

A Tunable Slow Light Device with Multiple Channels Based on Plasmon-Induced Transparency

Yiyuan Xie[1,2,3] · Junxiong Chai[1] · Yichen Ye[1] · Tingting Song[1] · Bocheng Liu[1] · Liangyi Zhang[1] · Yunchao Zhu[1] · Yong Liu[3]

Received: 6 October 2020 / Accepted: 29 December 2020 / Published online: 11 April 2021

Abstract

Slow light devices with buffering capability play a critical role in all-optical signal processing. In this paper, multiple slow light phenomena are implemented based on plasmon-induced transparency (PIT) in our device. The device mainly consists of dual tooth cavities coupled with stub resonators, respectively. Temporal coupled-mode theory model illustrates that the triple PIT phenomena can be achieved based on different formation mechanisms. The simulation results calculated by the finite-difference time-domain method reveal that significant slow light response occurs at two wavelength regions. In addition, the parameters of structure have an important influence on PIT response and slow light characteristics. Moreover, the separate manipulation of wavelength, transmission and group index at transparency peak can be achieved in different slow light channels by adjusting the structural parameters. This plasmonic device is of great significance for the design of optical networks on chips.

Keywords Slow light · Surface plasmon polaritons · Resonators · Plasmon-induced transparency · Transmission characteristics

Introduction

Electromagnetically induced transparency (EIT) is a quantum interference phenomenon between two different excitation pathways in a three-level atomic system, which can generate a narrow transparency window [1, 2]. It is generally accompanied with sharp dispersion near the transparency window [3]. This attractive phenomenon has various potential applications in the areas of optical data storage, ultrafast switching and slow light devices [4–6]. In particular, slow light devices can slow down the propagation speed of optical signals, temporarily store blocked optical signals and resolve resource conflicts in signals transmission [7, 8]. Moreover, the buffering is also required for synchronization, optical time-division multiplexing and optical beamforming [9]. Therefore, slow light propagation has been extensively studied [10, 11]. However, practical implementation of EIT is limited by strict conditions, such as low-temperature environments and stable gas lasers [12–14]. Fortunately, plasmon-induced transparency (PIT), an analogous EIT effect, has attracted the attention of researchers [15–17]. Compared with EIT, the PIT can remove rigorous implementation conditions. Furthermore, since surface plasmon polaritons (SPPs), a special kind of electromagnetic wave, have the capability of breaking classical diffraction limit, the PIT can be implemented in nanoscale structures [18–21].

Therefore, many slow light devices based on the PIT have been proposed to achieve slow light phenomena [22–25]. Among these devices of implementing PIT and slow light effects, for the metal-insulator-metal (MIM) waveguides having the advantages of ease fabrication, strong confinement to SPPs and acceptable propagation length, the MIM waveguides are widely employed [26–28]. For example, tunable slow light was analyzed in dual stubs coupled with MIM waveguide [2]. Slow light response was achieved in dual-

✉ Yiyuan Xie
yyxie@swu.edu.cn

1 School of Electronics and Information Engineering, Southwest University, Chongqing 400715, China

2 Chongqing Key Laboratory of Nonlinear Circuits and Intelligent Information Processing, Chongqing 400715, China

3 School of Optoelectronic Information, University of Electronic Science and Technology of Chengdu, Sichuan 611731, China

ring resonator-coupled MIM waveguide system [22]. A stub MIM waveguide coupled with a nanodisk resonator for PIT and slow-light effect was proposed [23]. Although these plasmonic devices have great performance, they can only be used to implement the PIT and slow light effect at a single wavelength. In order to solve the above problem, many plasmonic structures that can implement PIT response and slow light effect with multiple channels are investigated, such as dual coupled stub-nanodisks system [5], MIM stub coupled with two Fabry–Perots structure [24] and aperture-coupled cascade resonators [25]. These structures proposed further improve the integration of the device. However, how to individually manipulate the slow light characteristics at one of the channels without affecting the other channels, which is urgently needed in practical applications, is not discussed in detail.

To meet these demands, a slow light device mainly consisting of two tooth cavities coupled with stub resonators is proposed in this paper. The triple PIT responses are achieved at different wavelengths in the proposed device. The physical mechanisms of their formation are analyzed in detail using temporal coupled-mode theory (CMT) model. The simulation results calculated by finite-difference time-domain (FDTD) method reveal that significant slow light characteristics occurs at two of the wavelengths. Depending on the cause of the formation, we illustrate the methods of manipulating wavelength, transmission and group index at transparency peak for different slow light areas separately. The device proposed will pave the way for buffer technique in highly integrated optical systems.

Structure Model and Theoretical Analysis

A two-dimensional schematic diagram of the proposed plasmonic structure which mainly consists of dual tooth cavities coupled with stub resonators separately is shown in Fig. 1. The geometric parameters of the structure l_{t1}, l_{t2}, l_{s1} and l_{s2} are the lengths of the tooth$_1$, tooth$_2$, stub$_1$ and stub$_2$ resonators, respectively. The widths of waveguide, tooth cavities and stub resonators are denoted as w. Parameter D means the core-core separation between two tooth resonators, d_1 (d_2) represents the coupling distance between tooth$_1$ (tooth$_2$) cavity and stub$_1$ (stub$_2$) resonator. The refractive index of dielectric in waveguide and resonators is n. The background metal is supposed to be silver whose frequency-dependent relative permittivity can be characterized by the well-known Drude model [29]:

$$\varepsilon_m(\omega) = \varepsilon_\infty - \omega_p^2/[\omega(\omega + j\gamma)] \tag{1}$$

where $\varepsilon_\infty = 3.7$, $\omega_p = 9.1$ eV and $\gamma = 0.018$ eV are the dielectric constant of the infinite frequency, the bulk plasma

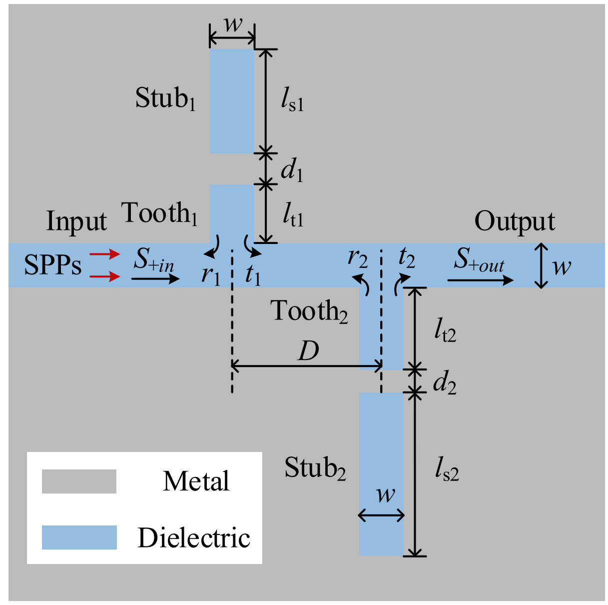

Fig. 1 Schematic diagram of the proposed plasmonic slow light device

frequency and the electron collision frequency, respectively. (Drude model with these parameter values can well describe the permittivity at infrared frequencies [30].) The angular frequency of the incident wave is denoted by ω. In this model, since the width of the plasmonic waveguide is much smaller than the wavelength of the incident light, only the TM_0 waveguide mode can propagate and dispersion relation for TM_0 mode in the MIM waveguide can be obtained by the following equations[31]:

$$(\varepsilon_m k_d) tanh(\frac{wk_d}{2}) + \varepsilon_d k_m = 0 \tag{2}$$

$$k_{d,m} = \sqrt{\beta^2 - \varepsilon_{d,m} k_0^2} \tag{3}$$

where ε_d, ε_m, k_d, k_m, respectively, represent the permittivities and propagation constants of the dielectric and metal. The wave vector β in the waveguide can be expressed as $\beta = k_0\, n_{eff}$, in which $k_0 = 2\pi/\lambda$ stands for the wave vector in vacuum and n_{eff} is the effective refractive index in plasmonic waveguide.

When the incident light is injected, the SPPs are formed on the metallic surfaces and propagate along bus waveguide. When resonance condition is satisfied, SPPs can be coupled directly to the tooth cavities from bus waveguide and coupled indirectly into the stub resonators through the tooth cavities. The resonance condition of tooth$_i$ cavity and stub$_i$ resonator ($i = 1, 2$) can be, respectively, described as[32, 33]:

$$2Re(N_{eff})l_{\text{ti}}\frac{2\pi}{\lambda_{tim}}+\Delta\phi_{ti}=(2m+1)\pi \quad (4)$$

$$2Re(N_{eff})l_{\text{si}}\frac{2\pi}{\lambda_{sin}}+\Delta\phi_{si}=2n\pi \quad (5)$$

where $Re(N_{eff})$ means the real part of the effective refractive index in the tooth and stub cavities, λ_{tim} and λ_{sin} are resonance wavelengths of tooth$_\text{i}$ cavity and stub$_\text{i}$ resonator, m is a non-negative integer and n is a positive integer. The additional phase shifts $\Delta\phi_{ti}$ and $\Delta\phi_{si}$ are caused by reflection on the interface of dielectric and metal in the tooth$_\text{i}$ cavity and stub$_\text{i}$ resonator, respectively.

Transmission characteristics of the structure can be investigated according to the CMT model. As shown in Fig. 1, t_1, r_1, t_2 and r_2 represent the transmission and reflection coefficients of the tooth$_1$ and tooth$_2$. For obtaining the transmission coefficients t_i and reflection coefficients r_i of the device, we first analyze the transmission characteristics of a single tooth cavity coupled with stub resonator. Figure 2 illustrates the cross section schematic diagram of single tooth cavity coupled with stub resonator.

The temporal evolution of the normalized amplitude a_i of the tooth$_\text{i}$ resonator can be written as[34]:

$$\frac{da_i}{dt}=(j\omega_i-k_{oi}-k_{wi}-k_{si})a_i+e^{j\varphi_{wi}}\sqrt{k_{wi}}(S^i_{+in}+S^i_{-in})+e^{j\varphi_{si}}\sqrt{2k_{si}}S^i_{+si} \quad (6)$$

where ω_i means the resonance frequency of tooth$_\text{i}$ resonator, k_{oi}, k_{wi} and k_{si} stand for decay rate due to internal loss in the tooth$_\text{i}$, the decay rate induced by the energy escape into the bus waveguide and stub$_\text{i}$ resonator, respectively. The phases of the coupling coefficients are denoted by φ_{wi} and φ_{si}. As shown in Fig. 2, $S^i_{\pm in}$ represent the amplitudes of the inputting waves in the MIM waveguide, subscript ± mean two propagating directions of waveguide modes. In addition, the amplitudes $S^i_{\pm si}$ of inputting and outgoing waves in the stub$_\text{i}$ resonator should satisfy a steady-state relation:

$$S^i_{-si}=-S^i_{+si}+e^{-j\varphi_{si}}\sqrt{2k_{si}}a_i \quad (7)$$

$$S^i_{+si}=\delta_i e^{j\phi_i}S^i_{-si} \quad (8)$$

where δ_i and $\phi_i=2l_{\text{si}}\omega Re(N_{eff})/c+\theta_i$ represent the amplitude attenuation and the phase difference between the incoming and outgoing waves of the stub$_\text{i}$ resonator, θ_i means the additional phase shift in the stub$_\text{i}$ resonator. In the linear system, the field everywhere oscillates as $e^{j\omega_i t}$ and $da_i/dt=j\omega_i a_i$. Since the light is only inputted into bus waveguide from the left port ($S^i_{-in}=0$), according to the above equations, amplitude a_i of the stub$_\text{i}$ resonator is derived as:

$$a_i=\frac{e^{j\varphi_{wi}}\sqrt{k_{wi}}S^i_{+in}}{j(\omega_i-\omega)+k_{oi}+k_{wi}+k_{si}-\frac{2k_{si}\delta_i e^{j\phi_i}}{1+\delta_i e^{j\phi_i}}} \quad (9)$$

Based on energy conservation, the amplitudes $S^i_{\pm out}$ of the outgoing waves can be expressed as:

$$S^i_{-out}=S^i_{-in}-e^{-j\varphi_{wi}}\sqrt{k_{wi}}a_i \quad (10)$$

$$S^i_{+out}=S^i_{+in}-e^{-j\varphi_{wi}}\sqrt{k_{wi}}a_i \quad (11)$$

According to the above equations, the transmission T_i of the single tooth cavity coupled with stub resonator structure can be deduced as:

$$T_i=\left|\frac{S^i_{+out}}{S^i_{+in}}\right|^2=\left|\frac{j(\omega_i-\omega)+k_{oi}+k_{si}\frac{1-\delta_i e^{j\phi_i}}{1+\delta_i e^{j\phi_i}}}{j(\omega_i-\omega)+k_{oi}+k_{wi}+k_{si}\frac{1-\delta_i e^{j\phi_i}}{1+\delta_i e^{j\phi_i}}}\right|^2 \quad (12)$$

Obviously, as coupling distance d_i increases, k_{si} will gradually decrease. When tooth$_\text{i}$ cavity and stub$_\text{i}$ resonator are no longer interaction ($k_{si}=0$), equation (12) is modified as:

$$T_s=\left|\frac{j(\omega_i-\omega)+k_{oi}}{j(\omega_i-\omega)+k_{oi}+k_{wi}}\right|^2 \quad (13)$$

When $\omega=\omega_i$, transmission T_s approximately equals 0 under the condition of $k_{oi}\ll k_{wi}$, which is consistent with the transmission of the band-stop filter based on SPPs. By comparing equation (12) and (13), it can be seen that due to the interaction between tooth$_\text{i}$ cavity and stub$_\text{i}$ resonator, the EIT-like response occurs, which means that a recess is generated at the original absorption peak and a transparency

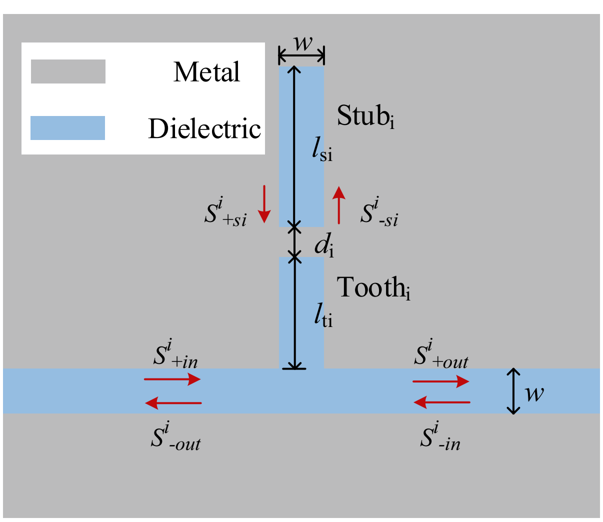

Fig. 2 Schematic diagram of single tooth cavity coupled with stub resonator

window is formed. Moreover, based on the above analyses, we can obtain the transmission and reflection coefficients of the single tooth$_i$ cavity coupled with stub$_i$ resonator as follows:

$$t_i = \frac{j(\omega_i - \omega) + k_{oi} + k_{si}\frac{1-\delta_i e^{j\phi_i}}{1+\delta_i e^{j\phi_i}}}{j(\omega_i - \omega) + k_{oi} + k_{wi} + k_{si}\frac{1-\delta_i e^{j\phi_i}}{1+\delta_i e^{j\phi_i}}} \tag{14}$$

$$r_i = \frac{k_{wi}}{j(\omega_i - \omega) + k_{oi} + k_{wi} + k_{si}\frac{1-\delta_i e^{j\phi_i}}{1+\delta_i e^{j\phi_i}}} \tag{15}$$

Consequently, feedback and transmitted waves of the ith tooth cavity can be expressed as following matrix:

$$\begin{bmatrix} S^i_{-in} \\ S^i_{+out} \end{bmatrix} = \begin{bmatrix} -\frac{r_i}{t_i} & \frac{1}{t_i} \\ 1 + \frac{r_i}{t_i} & \frac{r_i}{t_i} \end{bmatrix} \begin{bmatrix} S^i_{+in} \\ S^i_{-out} \end{bmatrix} \tag{16}$$

According to the above equation, the feedback and transmitted waves of the proposed device can be obtained as:

$$\begin{bmatrix} S_{-in} \\ S_{+out} \end{bmatrix} = \begin{bmatrix} -\frac{r_2}{t_2} & \frac{1}{t_2} \\ 1 + \frac{r_2}{t_2} & \frac{r_2}{t_2} \end{bmatrix} \begin{bmatrix} 0 & e^{j\theta'} \\ e^{-j\theta'} & 0 \end{bmatrix} \begin{bmatrix} -\frac{r_1}{t_1} & \frac{1}{t_1} \\ 1 + \frac{r_1}{t_1} & \frac{r_1}{t_1} \end{bmatrix} \begin{bmatrix} S_{+in} \\ S_{-out} \end{bmatrix} \tag{17}$$

where $\theta' = \omega Re(n_{eff})D/c$ is the phase difference between the 1st and 2nd tooth cavities. When the incident light is launched only from the left port in device ($S_{-in} = 0$), the transmission efficiency T at the output port can be derived as:

$$T = \left| \frac{S_{+out}}{S_{+in}} \right|^2 = \left| \frac{t_1 t_2}{1 - r_1 r_2 e^{j2\theta'}} \right|^2 \tag{18}$$

When the separation D is set to 0, the smallest device size and the maximum transmission can be obtained. The maximum transmission can be written as:

$$T_{max} = \left| \frac{S_{+out}}{S_{+in}} \right|^2 = \left| \frac{t_1 t_2}{1 - r_1 r_2} \right|^2 \tag{19}$$

According to the above analyses, we know that transmission characteristics of proposed device are not only related to interference between radiative (directly coupled to waveguide) resonators and subradiant (indirectly coupled to waveguide) resonators but also include phase coupling mechanism. In addition, from the previous derivation, working wavelengths can be selected by changing the lengths of tooth and stub cavities as shown in equation (4) and (5). Transmission of device can be manipulated by adjusting the coupling distance d_i since the coupling distances d_i are related to the transmission coefficients t_i and reflection coefficients r_i as illustrated in equation (12) and (13).

Results and Discussions

Transmission Characteristics

We take 2-D FDTD method to further investigate the transmission characteristics of the device. The mode source is introduced to excite fundamental TM mode of the waveguide and perfectly matched layer (PML) is utilized as boundary conditions. The spatial steps and temporal step are set as $\Delta x = \Delta y = 4$ nm and $\Delta t = \Delta x/1.43c$. First of all, the parameters of structure are set as $l_{t1} = 120$ nm, $l_{s1} = 260$ nm, $l_{t2} = 200$ nm, $l_{s2} = 420$ nm, $d_1 = 25$ nm and $d_2 = 20$ nm. In order to fix the characteristics of guided modes, the widths of waveguide and resonators are set as a constant (50 nm) in this paper. The dielectric embedded in the waveguide and resonators is regarded as air. Figure 3a shows the transmission spectra of the device calculated by the theory and simulation. As drawn in Fig. 3a, triple PIT windows can be observed and central wavelengths, respectively, are located at $\lambda_B = 855.9$ nm, $\lambda_D = 1114.5$ nm and $\lambda_F = 1314.3$ nm. The transmission efficiencies of transparency peak reach 50%, 90% and 42%, respectively, between the four resonance dips at $\lambda_A = 819.1$ nm, $\lambda_C = 897.6$ nm, $\lambda_E = 1260.6$ nm and $\lambda_G = 1364.9$ nm, which are typical representation of PIT.

The field distributions of H_Z at the transmission peaks and resonance dips represented by A, B, C, D, E, F and G are sketched in Figs. 3b-h. According to the previous theoretical analysis and field distributions, two transparency windows are formed by interaction between tooth$_i$ cavity and stub$_i$ resonator: transparency window with a central wavelength at 855.9 nm (PIT$_1$ window) and transparency window with a central wavelength at 1314.3 nm (PIT$_2$ window). The formation of transparency window with a central wavelength at 1114.5 nm (PIT$_3$ window) originates from the phase interference between the two tooth cavities. Moreover, PIT$_1$ (PIT$_2$) is mainly formed by the interaction of tooth$_1$ (tooth$_2$) cavity and stub$_1$ (stub$_2$) resonator. Therefore, the transmission characteristics of PIT$_1$ window or PIT$_2$ window can be individually manipulated by adjusting the structural parameters.

Slow Light Effect

The results calculated by FDTD method reveal that phase shift exhibits a sharp dithering at PIT$_1$ and PIT$_2$ windows, which means that obvious slow light phenomenon appeared at the two transparency windows. The group index n_g of the device affects buffering time of signal, and physical significance of group index not only includes the meaning

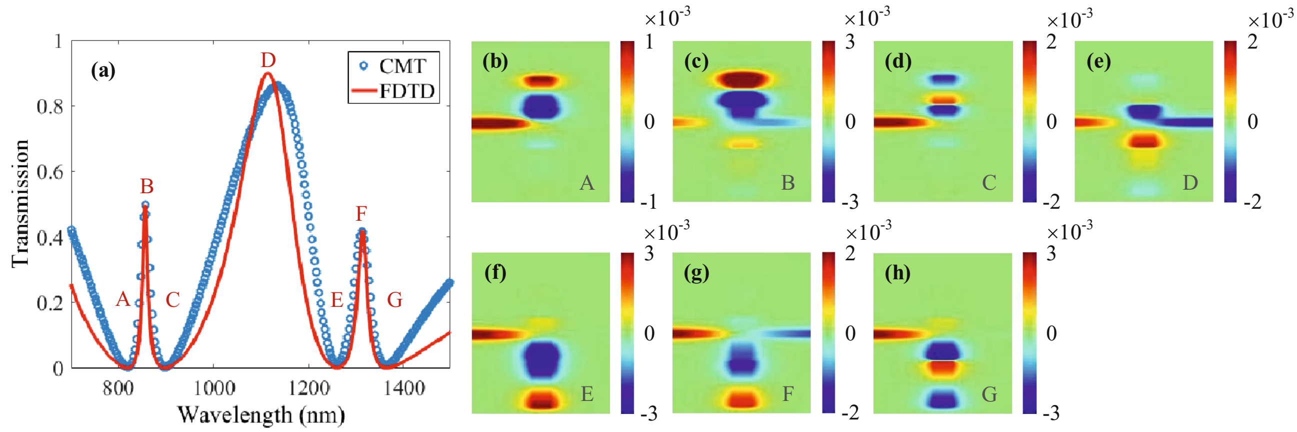

Fig. 3 **(a)** Transmission spectra at output port of proposed device calculated by the CMT and FDTD methods. Filed distributions of H_Z in the proposed device with the incident light wavelength of **(b)** 819.1 nm, **(c)** 855.9 nm, **(d)** 897.6 nm, **(e)** 1114.5 nm, **(f)** 1260.6 nm, **(g)** 1314.3 nm and **(h)** 1364.9 nm

of refractive index but also reflects the dispersion properties. Therefore, the slow light characteristic can be expressed by the group index, which is denoted by following equation:

$$n_g = \frac{c}{v_g} = \frac{c}{L}\tau_g = \frac{c}{L}\frac{d\psi(\omega)}{d\omega} \tag{20}$$

where v_g, τ_g and L are group velocity, optical delay time and the length of the plasmonic structure, respectively. The transmission phase shift $\psi(\omega)$ is a function of angular frequency ω, which can be obtained by $\psi(\omega) =$ angular (S_{+out}/S_{+in}).

We numerically investigated the slow light behavior of the device with the length L is set to 500 nm. Figure 4a shows the transmission phase shift at PIT_1 window. The phase jitter at PIT_1 window results in delay time at PIT_1 window and the delay time of peak B reaches maximum value 0.06 ps, as depicted in Fig. 4b. Based on equation (20), the group index at PIT_1 window is plotted, as shown in Fig. 4c. The strong dispersion around the transparency window leads to high group indices and maximum group index at peak of PIT_1 window is over 34. Similarly, Figs. 4d-f illustrate the phase shift, delay time and group index at PIT_2 window. The results show that the maximal group delay time and group index reach 0.074 ps and 44 at peak of PIT_2 window, respectively. Therefore, different slow light areas are achieved at commonly used wavebands.

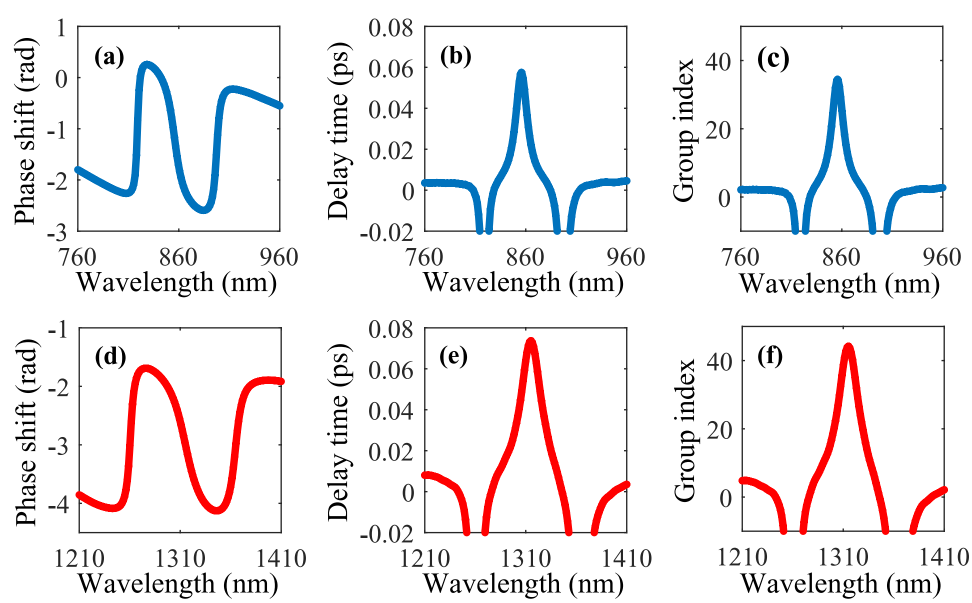

Fig. 4 **(a)** Transmission phase shift, **(b)** delay time and **(c)** group index at the PIT_1 window. **(d)** Transmission phase shift, **(e)** delay time and **(f)** group index at the PIT_2 window

Influence of Structural Parameters

As we have analyzed in the previous theory, the controllability of the transmission characteristics can be achieved by adjusting the lengths of resonators and coupling distances, for example, selected operating wavelengths and variable transmissions. For verifying the previous analyses, sweeps of the numerical parameters are performed. Above all, the impacts of the length l_{t1} and length l_{s1} on the transmission characteristics are analyzed. The length l_{t1} is taken from 110 nm to 130 nm with an interval of 5 nm. In order to ensure the detuning state of the resonant wavelength between tooth$_1$ and stub$_1$ resonator remains invariable, the length l_{s1} satisfies the formula $l_{s1} = 2l_{t1} + a$. The parameter a is set to 20 nm, and other parameters are fixed to $l_{t2} = 200$ nm, $l_{s2} = 420$ nm, $d_1 = 25$ nm and $d_2 = 20$ nm. As the length l_{t1} and length l_{s1} increase, the variation of transparency peak wavelengths at PIT$_1$ and PIT$_2$ windows is plotted in Fig. 5a. It is noteworthy that the central wavelength of PIT$_1$ window exhibits a red-shift with the increase of length l_{t1} and length l_{s1}, which is basically a linear relationship. Meanwhile, the resonance wavelength of PIT$_2$ is barely changed. So, we can manipulate the central wavelength of PIT$_1$ window without affecting PIT$_2$ by changing the length l_{t1} and length l_{s1}.

Then, we investigate the influence of the length l_{t2} and length l_{s2} on the transmission characteristics. Length l_{t2} increases from 190 nm to 210 nm with the step size of 5 nm. The length l_{s2} is expressed as $l_{s2} = 2l_{t2} + a$ and the other parameters remain unchanged. Figure 5b illustrates the variation of central wavelengths at PIT$_1$ and PIT$_2$ windows. As the Length l_{t2} and Length l_{s2} increase, central wavelength of PIT$_2$ window exhibits red-shift while resonance wavelength of PIT$_1$ has almost no movement. Therefore, by adjusting the length l_{t2} and length l_{s2}, the transparency peak wavelength of PIT$_2$ can be individually manipulated.

As we all know, transmission and group index are important indicators for a slow light device. Next, we explore the effects of coupling distance d_1 on the transmission and group index. The coupling distance d_1 is varied from 10 nm to 35 nm in steps of 5 nm whereas other parameters are kept fixed. Figure 6a depicts the relationship between transmission of transparency peak at PIT$_1$ and coupling distance d_1. As the coupling distance d_1 increases, the transmission at transparency peak of PIT$_1$ gradually decreases. However, the group index at transparency peak of PIT$_1$ gradually increases, as drawn in Fig. 6b. There is a trade-off problem between the group index and the transmission through calculation. In order to achieve appropriate transmission and higher group index at the same time, the coupling distance d_1 is set to 25 nm in this paper. In addition, it can be observed from Figs. 6a, b that the transmission and the group index at central wavelength of PIT$_2$ window are hardly affected when coupling distance d_1 increases. This provides a method of manipulating the transmission and group index of central wavelength at PIT$_1$ window without affecting the slow light characteristics of PIT$_2$ window.

Finally, the relationship between the coupling distance d_2 and slow light characteristics are researched. The coupling distance d_2 is taken from 10 nm to 35 nm with an interval of 5 nm, while the other parameters remain invariable. As the coupling distance d_2 increases, the variation in the transmission and group index at transparency peak of PIT$_1$ and PIT$_2$ is shown in Figs. 7a, b. Contrary to the consequence of adjusting coupling distance d_1, when the coupling distance d_2 increases, the transmission and group index at transparency peak of PIT$_1$ are barely influenced. Meanwhile, the transmission and group index at central wavelength of PIT$_2$ window present a tendency to decrease and increase, respectively. Therefore, we can manipulate the transmission and group index at transparency peak of PIT$_2$ separately.

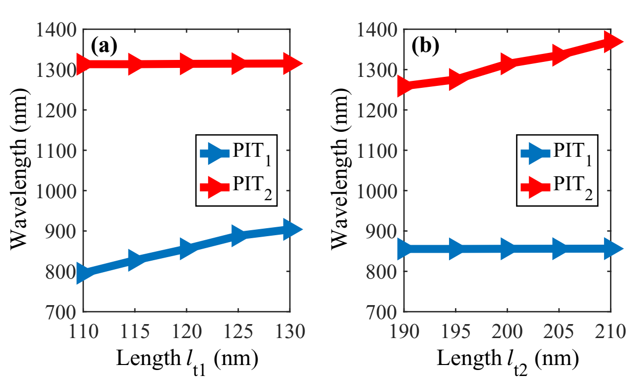

Fig. 5 **(a)** Variation tendency of the transparency peak wavelengths at PIT$_1$ and PIT$_2$ windows as length l_{t1} and length l_{s1} increase. **(b)** Variation tendency of the transparency peak wavelengths at PIT$_1$ and PIT$_2$ windows as length l_{t2} and length l_{s2} increase

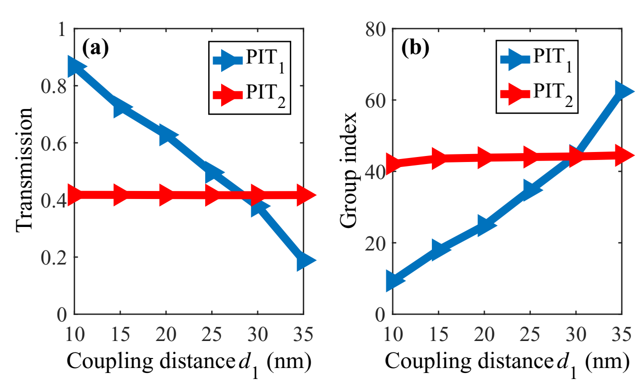

Fig. 6 **(a)** The transmission at peak of PIT windows as functions of coupling distance d_1. **(b)** The relationship between group index at peak of PIT windows and the coupling distance d_1

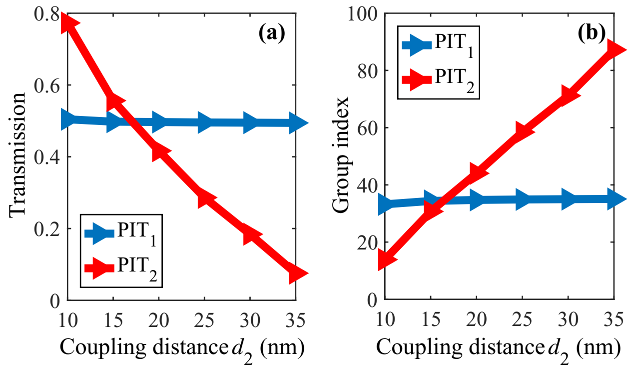

Fig. 7 **(a)** The transmission at peak of PIT windows as functions of coupling distance d_2. **(b)** The relationship between group index at peak of PIT windows and the coupling distance d_2

The coupling distance d_2 is set to 20 nm for obtaining higher transmission and group index simultaneously in this paper.

Conclusion

In summary, we proposed a novel plasmonic structure mainly consisting of two tooth cavities coupled with stub resonators, respectively. Triple PIT windows are implemented based on different formation mechanisms and the reasons of formation are analyzed in detail using CMT model. Simulation results calculated by the FDTD method demonstrate that the obvious slow light responses at PIT_1 and PIT_2 windows are achieved. In addition, we can separately manipulate the transmission characteristics of PIT_1 and PIT_2 windows, including the wavelength, transmission and group index of transparency peak. The proposed plasmonic slow light device has many potential applications in highly integrated photonic loop.

Author Contributions Yiyuan Xie contributed to conceptualization, supervision and writing—review. Junxiong Chai provided methodology and software and performed writing—original draft, and writing—editing. Yichen Ye, Tingting Song, Bocheng Liu, Liangyi Zhang, Yunchao Zhu and Yong Liu performed writing—review.

Funding This work was supported by the Natural Science Foundation of Chongqing City under Grant cstc2016jcyjA0581, by the Postdoctoral Science Foundation of China under Grant 2016M590875, by the Fundamental Research Funds for the Central Universities under Grant XDJK2018B012.

Data Availability All data generated or analyzed during this study are included in this article.

Compliance with Ethical Standards

Conflicts of Interest The authors declare that they have no conflict of interest.

Consent to Participate Informed consent was obtained from all participants.

Consent to Publish Informed consent for publication was obtained from all authors.

References

1. Ye J, Wang F, Liang R, Wei Z, Meng H, Zhong J, Jiang L (2016) Plasmon induced transparency in loop-stub resonator-coupled waveguide systems. Opt Commun 370:36–42
2. Wang G, Zhang W, Gong Y, Liang J (2015) Tunable slow light based on plasmon-induced transparency in dual-stub-coupled waveguide. IEEE Photonics Technol Lett 27(1):89–92
3. Zafar R, Salim M (2015) Achievement of large normalized delay bandwidth product by exciting electromagnetic-induced transparency in plasmonic waveguide. IEEE J Quantum Electron 51(10):7200306
4. Li X, Xie R, Li W, Li Z, Gu E, Niu L, Guo S (2019) Adjustable electromagnetically induced transparency effect based on graphene surface plasmon. Superlattices Microstruct 128:342–348
5. Wang Q, Meng H, Huang B, Wang H, Zhang X, Yu W, Tan C, Huang X, Li S (2016) Dual coupled-resonator system for plasmon-induced transparency and slow light effect. Opt Commun 380:95–100
6. Lu H, Liu X, Mao D (2012) Plasmonic analog of electromagnetically induced transparency in multi-nanoresonator-coupled waveguide systems. Phys Rev A 85(5):053803
7. Liu D, Sun S, Yin X, Sun B, Sun J, Liu Y, Li W, Zhu N, Li M (2019) Large-capacity and low-loss integrated optical buffer. Opt Express 27(8):11585–11593
8. Liu W, Romeira B, Li M, Guzzon RS, Norberg EJ, Parker JS, Coldren LA, Yao JP (2016) A wavelength tunable optical buffer based on self-pulsation in an active microring resonator. J Lightwave Technol 34(14):3466–3472
9. Zhou L, Wang X, Lu L, Chen J (2018) Integrated optical delay lines: a review and perspective. Chin Opt Lett 16(10):101301
10. Wheeler NV, Light PS, Couny F, Benabid F (2010) Slow and superluminal light pulses via EIT in a 20-m acetylene-filled photonic microcell. J Lightwave Technol 28(6):870–875
11. Lukin MD, Imamoglu A (2001) Controlling photons using electromagnetically induced transparency. Nature 413(6853):273–276
12. Gu J, Singh R, Liu X, Zhang X, Ma Y, Zhang S, Maier SA, Tian Z, Azad AK, Chen HT, Taylor AJ, Han J, Zhang W (2012) Active control of electromagnetically induced transparency analogue in terahertz metamaterials. Nat Commun 3:1151
13. Shi X, Su X, Yang Y (2015) Enhanced tunability of plasmon induced transparency in graphene strips. J Appl Phys 117(14):143101
14. Chai Z, Hu X, Zhu Y, Sun S, Yang H, Gong Q (2014) Ultracompact chip-integrated electromagnetically induced transparency in a single plasmonic composite nanocavity. Adv Opt Mater 2(4):320–325
15. Yao G, Ling F, Yue J, Luo Q, Yao J (2016) Dynamically tunable graphene plasmon-induced transparency in the terahertz region. J Lightwave Technol 34(16):3937–3942
16. Xie Y, Ye Y, Liu Y, Wang S, Zhang J, Liu Y (2018) Synchronous slow and fast light based on plasmon-induced transparency and absorption in dual hexagonal ring resonators. IEEE Trans Nanotechnol 17(3):552–558
17. Zhang ZD, Wang RB, Zhang ZY, Tang J, Zhang WD, Xue CY, Yan SB (2017) Electromagnetically induced transparency and refractive index sensing for a plasmonic waveguide with a stub coupled ring resonator. Plasmonics 12(4):1007–1013

18. Barnes WL, Dereux A, Ebbesen TW (2003) Surface plasmon subwavelength optics. Nature 424:824–830
19. Armaghani S, Khani S, Danaie M (2019) Design of all-optical graphene switches based on a mach-zehnder interferometer employing optical kerr effect. Superlattices Microstruct 135:106244
20. Gramotnev DK, Bozhevolnyi SI (2010) Plasmonics beyond the diffraction limit. Nat Photonics 4(2):83–91
21. Genet C, Ebbesen TW (2007) Light in tiny holes. Nature 445(7123):39–46
22. Zhan S, Li H, Cao G, He Z, Li B, Yang H (2014) Slow light based on plasmon-induced transparency in dual-ring resonator-coupled MDM waveguide system. J Phys D: Appl Phys 47(20):205101
23. Huang B, Meng H, Wang Q, Wang H, Zhang X, Yu W, Tan C, Huang X, Wang F (2016) Plasmonic-induced transparency and slow-light effect based on stub waveguide with nanodisk resonator. Plasmonics 11(2):543–550
24. Yun B, Hu G, Cong J, Cui Y (2014) Plasmon induced transparency in metal-insulator-metal waveguide by a stub coupled with F-P resonator. Mater Res Express 1(3):036201
25. Zhang Z, Yang J, He X, Han Y, Zhang J, Huang J, Chen D, Xu S (2018) Plasmon-induced transparency based on aperture-coupled cascade resonators without gap. Superlattices Microstruct 123:138–143
26. Hosseini A, Massoud Y (2007) Nanoscale surface plasmon based resonator using rectangular geometry. Appl Phys Lett 90(18):181102
27. Rakhshani MR, Mansouri-Birjandi MA (2017) High sensitivity plasmonic refractive index sensing and its application for human blood group identification. Sens Actuators B 249:168–176
28. Zhai X, Wang L, Wang LL, Li XF, Huang WQ, Wen SC, Fan DY (2013) Tuning bandgap of a double-tooth-shaped MIM waveguide filter by control widths of the teeth. J Opt 15(5):055008
29. Wang G, Lu H, Liu X, Mao D, Duan L (2011) Tunable multi-channel wavelength demultiplexer based on MIM plasmonic nanodisk resonators at telecommunication regime. Opt Express 19(4):3513–3518
30. Han Z, Bozhevolnyi SI (2011) Plasmon-induced transparency with detuned ultracompact Fabry-Perot resonators in integrated plasmonic devices. Opt Express 19(4):3251–3257
31. Wang Y, Xie Y, Ye Y, Du Y, Liu B, Zheng W, Liu Y (2018) Exploring a novel approach to manipulating plasmon-induced transparency. Opt Commun 427:505–510
32. Feng Y, Liu Y, Wang X, Dong D, Shi Y, Hua S, Zhang H, Tang L (2016) Compact nanofilters based on plasmonics waveguide with archimedes' spiral nanostructure. IEEE Photonics J 8(5):4802908
33. Lu H, Liu X, Gong Y, Mao D, Wang G (2011) Analysis of nano-plasmonic wavelength demultiplexing based on metal-insulator-metal waveguides. J Opt Soc Amer B 28(7):1616–1621
34. Lu H, Liu X, Wang G, Mao D (2012) Tunable high-channel-count bandpass plasmonic filters based on an analogue of electromagnetically induced transparency. Nanotechnol 23(44):444003